Analyzing $CD8^+$ Cytotoxic T Lymphocyte Migration in The Complex Pancreatic Ductal Adenocarcinoma Tumor Microenvironment

A Thesis

SUBMITTED TO THE FACULTY OF THE

UNIVERSITY OF MINNESOTA

BY

Hongrong Zhang

IN PARTIAL FULFILLMENT OF THE REQUIREMENTS

FOR THE DEGREE OF MASTER OF SCIENCE

ADVISOR:

Dr. Paolo P. Provenzano

May 2021

Acknowledgment

I would first like to express my deepest gratitude towards my advisor and mentor, Dr. Paolo Provenzano, for his continuous support and guidance throughout my journey at the University of Minnesota. Dr. Provenzano's passion and dedication to combating cancer have inspired and motivated me to complete the following work and continue my graduate study.

I would also like to thank my fellow lab mates for welcoming me to the lab and teaching me the skills and techniques for conducting my experiments. Mackenzie Callaway, Rachel Hessuer, and Rachel Edwards, thank you for introducing me to the lab, teaching me the techniques needed for my experiments, helping me troubleshooting problems, and offering advice, both personal and professional, when I needed them. Nelson Rodriguez, thank you for sharing your experience and knowledge to help me set up the experiments and setting up meetings to answer my questions. Dr. Amanda Salzwedel, thank you for training me on how to take care of the animals and have always been so kind to me. Dr. Alexandra Crampton, thank you for looking out for me and encouraging me to look forward whenever I had doubts or frustrated by failed experiments. Jon Zettervall, thank you for taking such good care of the lab and making sure we have everything needed for the experiments. It has been a very challenging time with COVID-19, and this work would not have been possible without all of your supports and encouragement. Thank you.

Last but not least, I would like to thank my parents, Changshou Zhang and Shujun Liu, and my sister, Jinrong Zhang, for their unconditional love and support. Your hard works and resilience have taught me to never gave up. I would not be the person I am today without

their constant encouragement. I would like to thank my special one, Guhan, for always be there for me and pushing me forward. My two adorable cats, Fidget and Phoenix, for being the sweetest cats one could only dream of and bring so much joy to my life.

All of you have given me the strength and courage needed to navigate through graduate school and life.

Dedication

I would like to dedicate this work to my parents, Changshou Zhang and Shujun Liu, and my sister Jinrong Zhang, for always be my rock.

Abstract

Pancreatic ductal adenocarcinoma (PDAC) remains one of the deadliest cancer types and is estimated to cause more than 432,242 death per year in 2018. Despite increased knowledge in cancer biology and advances in diagnosis tools, most patients were diagnosed at the malignant stage, unsuitable for surgical resection. Moreover, current treatment options like chemotherapy and radiation therapy have limited effect at the malignant stage and only serve as palliative care. Recently, immunotherapy like CAR-T cell therapy has gained great success in some cancer types. To perform the antitumor activities, T cells need to recognize tumor antigens by either establishing contacts with cancerous cells or antigen-presenting cells, which depends on a series of migratory steps from entry to the tumor to the locating of the malignant cells. The dense stroma associated with PDAC creates a great challenge for T cells to effectively migrate in the tumor microenvironment (TME). Also, the mechanism for T cell navigation and migration is not well understood. Here we presented a rapid and cost-effective method to fabricate 3D collagen gel matrix that closely assembles the remodeled extracellular matrix (ECM) in PDAC, allowing high throughput studies. To fully recapitulate the naïve TME, tumor slices from the KPCT genetically engineering PDAC mouse model that shares many of the disease characteristics of human PDAC can be prepared and cultured in an organotypic culture insert for up to six days while maintaining tissue integrity and cell viability. $CD8^+$ can be isolated from tumor-bearing KPC/KPCT mice and activated using Dynabeads T cell activator. Fully activated $CD8^+$ can then be seeded on top of the tumor slice, and attached/infiltrated T cell migration can be monitored using time-lapse imaging utilizing multiphoton laser scanning microscope (MPLSP), and tumor collagen stroma can be virtualized using second

harmonic generation (SHG). Additionally, Trackmate was used to track the cytotoxic T lymphocyte migrations in the TME. The 3D speed and motility of the T cells were further analyzed in carcinoma cell-rich and stroma-rich regions of the KPCT TME. Our data suggested that T cell speed and motility both increased significantly in the carcinoma-rich region, where collagen fibers are loosely connected, than that of the stroma-rich region. Taken together, the live imaging approach combined with quantitative analysis allows us to gain insight into T cell migration in the complex 3D TME and form new therapeutic approaches.

Table of Contents

List of Figures

List of Movies

Movie 1: Overlaid mCD8+ T cells (green) migration trajectories on KPCT tumor slice (tdTomato carcinoma cell: red; collagen: grey) for 45 minuets, shown in maximum intensity projection (MIP) of a 75 μm z-stack.

Movie 2-4: Live imaging of mCD8+ T cells (green) migrating on carcinoma-rich regions of the KPCT tumor slices (tdTomato carcinoma cell: red; collagen: grey) for 45 minutes, shown in MIP of a 75 μm z-stack.

Movie 5-8: Live imaging of $mCD8^{+}$ T cells (green) migrating on stroma-rich regions of the KPCT tumor slices (tdTomato carcinoma cell: red; collagen: grey) for 45 minutes, shown in MIP of a 75 μμ z-stack.

List of Abbreviations

PDAC: Pancreatic Ductal Adenocarcinoma

ECM: extracellular matrix

GEMM: Genetically engineered mouse model

DMEM: Dulbecco's Modified Eagle Medium

MIP: Maximum intensity projection

KPC: *KrasG12D/+;p53R172H/+;Pdx1-Cre*

KPCT: *KrasG12D/+;p53R172H/+;Pdx1-Cre;ROSATdtomato/+*

SHG: second harmonic generation

MPLSM: Multiphoton laser scanning microscopy

STT: stroma-targeted therapy

TME: tumor microenvironment

Chapter 1: Introduction

1.1 Epidemiology of Pancreatic Cancer

Pancreatic cancer is the most lethal common cancer type with a five-year relative survival rate of 8% (Saad et al., 2018). It is the 11th most common cancer but the 7th leading cause of cancer-related death across the world (McGuigan et al., 2018). In 2018, the GLOBOCAN estimated 458,918 people diagnosed with pancreatic cancer per year and causing 432,242 deaths, which accounts for 4.5% of all cancer-related deaths (Rawla et al., 2019). Despite advances in early diagnostic tools and increased knowledge of potential risk factors, most patients (80% - 85%) were still diagnosed at the malignant stage, unsuitable for surgical resection(Siegel et al., 2014). Even in patients who underwent resection, the recurrence rate is extremely high, and the 5-year survival rate is 25% at best (Zhang et al., 2018). Despite this high incident and high mortality rate, the cause for pancreatic cancer is still unknown, and treatments remain ineffective for the malignant stage (Schneider et al., 2005).

1.2 Pancreatic Ductal Adenocarcinoma

Most pancreatic cancer can be divided into two groups: pancreatic ductal adenocarcinoma (PDAC), which accounts for more than 85% of the cases and occurs in the exocrine glands of the pancreas, and pancreatic neuroendocrine tumor (PanNET), which is far less common and accounts for less than 5% of the cases (Rawla et al., 2019). Despite the tremendous scientific effort and increasing knowledge in PDAC at the cellular level, the survival rate hasn't improved much during the last decades (Schneider et al., 2005). One of the most important factors of pancreatic tumors is their ability to induce a highly fibrotic stroma.

The interstitial pressure of the tumor is consequently increased, and the tumor's vasculature becomes compressed (Li et al., 2019). In some pancreatic tumors, the total stromal volume can take up to 90% (Xie & Xie, 2015). This dense stroma creates a physical and biological barrier for any drug particles to pass through.

1.3 PDAC Treatments

Treatment for pancreatic cancer varies depending on the stage of the disease and where the tumor is located. Surgery, chemotherapy, radiation therapy, or a combination of these treatments are also possibilities (Kamisawa et al., 2016). Even though surgery can be successful when cancer is detected early enough, it has several disadvantages, including an elevated chance of bleeding and inflammation, as well as nausea and vomiting (Hafezi-Nejad et al., 2018). Aside from that, patients can experience nutrient deficiencies, diabetes, delayed gastric emptying, and other issues. In addition, the operation necessitates a lengthy treatment period that involves several days in the hospital and several weeks at home (Hafezi-Nejad et al., 2018). Chemotherapy is another treatment option for cancer patients. It is usually taken intravenously or orally. The treatment usually involves a combination of chemotherapeutic drugs or is usually given in combination with radiation therapy (chemoradiation). Chemoradiation is used if the cancer is aggressive and has metastasized to other organs (Lambert et al., 2019). Chemotherapy helps to reduce the size of the tumor and is used to prevent the reoccurrence of cancer after surgery. In the case of advanced cancer, chemotherapy is usually used as a form of palliative care to prolong a person's life for few months. For patients unsuitable for surgical resection, chemotherapy remains the standard care. The palliative chemotherapeutic drug, Gemcitabine, has been used to treat advanced cases of pancreatic cancer, though many cases became resistant to it (Burris III

et al., 1997). Recently, in combination with Gemcitabine, nab-Paclitaxel has become the new standard of care for metastatic pancreatic cancer but only slightly improved patient survival outcomes (Goldstein et al., 2015).

1.4 PDAC Immune Microenvironment

PDAC is one of the most stroma-rich cancer, making it difficult for drugs and effector immune cells to infiltrate (Watt & Kocher, 2013). The dense stroma is also heterogeneous and contains cellular and acellular components like fibroblasts, myofibroblasts, stellate cells, immune cells, blood vessels, endothelial cells, nerve cells, extracellular matrix (i.e., collagen, fibrinogen, hyaluronan, and fibrin), and a variety of proteins, enzymes, and growth factors (Rucki & Zheng, 2014). The dense stroma fibrosis in PDAC has long been thought to prevent any significant and specific immune response within the tumor. However, immunohistochemistry has revealed as early as 1998 that an enriched T cell population has infiltrated into PDAC compared to the normal pancreas (Emmrich et al., 1998). Those T cells can be characterized as either CD4 positive or CD8 positive (Emmrich et al., 1998). CD4 is a surface marker found on helper T cells and regulatory T cells, while CD8 is a surface marker for cytotoxic killer T cells (Seo & Pillarisetty, 2017). Even though those intratumoral effector T cells maintain their ability to activate inflammation, often, they became exhausted and trapped inside the dense stroma (von Bernstorff et al., 2001). In addition, the infiltration of immunosuppressive leukocytes, desmoplastic reaction with multiple cell types, and the inherent immunosuppressive molecular factors in the ECM create a hostile immune microenvironment (Clark et al., 2007).

1.5 Models to Study PDAC

Several models are available to study PDAC ranging from the 2-3D cell culture matrixes, cell lines, synthetic tumor xenografts to genetically engineered mouse models (GEMM) and tumor slices. Cell lines and monolayer cultures are cost-effectively and useful for high-throughput studies but lack the ability to fully capture the in vivo molecular integrations and the complex tumor microenvironment (Behrens et al., 2017). On the other hand, GEMM has a higher pathological relevance and can faithfully recapitulate key progress observed in human disease. The first GEMM for PDAC was produced by modifying genes associated with PDAC in the mouse genome (Behrens et al., 2017). In 2001, the generation of the K-rasLSL.G12D mouse allowed tissue-specific K-ras mutation expression in the endogenous mouse locus (Hingorani et al., 2003). Later, the K-rasLSL.G12D mice were crossed with PDX-Cre (referred to as the KC model) to target K-rasG12D specifically to the pancreases. The KC mice started developing early pancreatic intraepithelial neoplasia (PanIn) lesions by eight weeks of age, and a subset of those mice eventually developed PDAC with a median survival of 14 months (Westphalen & Olive, 2012). To accelerate tumor development, the p53R172H mutation was incorporated to generate the KPC mice model with a median survival of 5.5 months. In addition, around 80% of KPC mice develop metastases similar to human PDAC patients and sharing many of the immunohistochemical markers with human PDAC (Westphalen & Olive, 2012) (Paolo P. Provenzano et al., 2012). KPC mice can be crossed with mice bearing the tdTomato reporter strain to generate the KPCT murine model to better virtualize carcinoma cells (Stopczynski et al., 2014).

Recently, tissue slice culture has gained great interest in studying cancer biology (Davies et al., 2015). Its ability to capture the tumor architecture and maintain cellular viability has

allowed for studies like toxicity, drug metabolism, mechanism of resistance, and gene therapy testing in multiple cancer types, including the liver, lung, kidney, breast, and pancreas (de Kanter et al., 2002)(Marciniak et al., 2013)(Gerlach et al., 2014) . In the 2016 study by Jiang et al., human PDAC tumor slice culture was cultured using an organotypic culture system and verified that it could maintain the baseline morphology, surface area, and microenvironment for at least six days in culture (X. Jiang et al., 2017). Thus, tumor slices from KPC/KPCT mice can be a useful tool to study the dynamic immune interactions in the complex PDAC tumor microenvironment.

Chapter 2: Material and Methods:

2.1 3D Collagen Gel Fabrication and Quantification

3D collagen matrix was prepared as previously described (Ray et al., 2017). Briefly, high concentration rat tail collagen type I (Life Sciences, Corning, USA) was neutralized with 1mM HEPE in 2X PBS at a 1:1 ratio. Serum-free DMEM, either at room temperature or prewarmed to 37˚C, was added to produce a 3 mg/ml final collagen concentration. 350 µL of collagen solution was pipetted into each well of a standard 24-well culture plate and was left undisturbed for 30 minutes at room temperature to allow polymerization before moving into a 37˚C, 5% CO2 incubator. The gel was then overlaid with 1 mL of serum-free DMEM per well and continued to incubate at 37˚C overnight. Collagen gels form completely around 16 hours. After complete polymerization, the gel can be floated to allow transportation using a small pipette tip to detach from the sides of the well, follow by gently swirl and tap to detach from the bottom of the well. Collagen fiber quantification was analyzed using CT-FIRE (Bredfeldt, Liu, Pehlke, et al., 2014) and CurveAlign (Bredfeldt, Liu, Conklin, et al., 2014) as described before for fiber extraction and alignment measurement, respectively (Liu et al., 2017). Briefly, CT-FIRE uses the curvelet transform to denoise the SHG image and enhance the fiber edges, followed by a fiber tracking algorithm (FIRE) to extract individual collagen fibers. CurveAlign can further analyze the resulted fiber network to determine the alignment of fibers with respect to each other, termed "alignment coefficient" ranging from 0 to 1, where 1 indicates perfectly aligned fibers (Liu et al., 2017).

2.2 Mouse CD8+ T Cell Isolation, Activation, and Expansion

Mouse cytotoxic CD8+ T lymphocytes were extracted from tumor-bearing KPCT genetically engineered mice spleens using the EasySep $CD8^+$ T Cell Isolation Kit (STEMCELLTM Technologies Inc., USA), following the manufacture's recommendation with slight modification. Briefly, the mouse spleen was macerated using a springe plunger inside a 70 µm nylon cell strainer and rinsed with 10 mL of 1X PBS supplemented with 2% FBS and 100 mM EDTA. The sample was spined down at 300 g for 10 minutes and resuspended at 1 x 10^8 in 1X PBS supplemented with 2% FBS and 100 mM EDTA. $CD8^+$ T lymphocytes were negatively selected using the isolation kit following the manufacture's recommendation. 10% more of the recommended reagents were used for a higher yield and purity. Isolated $CD8^+$ T cells were cultured and activated using the Dynabeads Mouse T-Activator CD3/CD28 (ThermoFisher Scientific, MA), following the manufacturer's recommendation with slight modification. Briefly, 1 x 10^5 cells were cultured with 2.5 µL of the Dynabeads magnetic beads in ImmunoCult™-XF T cell expansion medium (STEMCELLTM Technologies Inc., USA), supplemented with 30 U/ml of interleukin 2 (IL-2) (STEMCELLTM Technologies Inc., USA) for at least four days before magnetic separation of the beads. Activated T cells can be used immediately or frozen down at -80 ˚C in FBS with 15% DMSO. T cells were frozen down at approximately1 ˚C per minute using Mr.Frosty™ (ThermoFisher Scientific, MA) for optimal cell preservation. Thaw activated T cells in 37 ˚C water bath for 2 to 3 minutes and washed cells in 10 mL fresh Immunocult media to remove excessive DMSO in the medium. Thawed T cells were allowed to recover in fresh Immunocult medium supplemented with 200 U/ml IL-2 (STEMCELLTM Technologies Inc., USA) for at least 24 hours before subsequent

experiments. All animal and cell work were approved by the University of Minnesota Institutional Biosafety Committee and followed institutional and NIH guidelines.

2.3 Cell Purity Analysis using Flow Cytometry

Isolated mouse $CD8^+$ T cells were analyzed using fluorescence-activated cell sorting (FACS) to ensure high purity. Briefly, aliquots of the non-depleted cell population, freshly harvested from the mouse spleen, and depleted cell population, isolated using the EasySep $CD8^+$ T cell isolation kit, were resuspended in 1X PBS and were either stained with CD8α antibody (STEMCELLTM Technologies Inc., USA), or without, followed by incubation on ice for one hour, protected from light. Incubated cell samples were run through the flow cytometer (BD Bioscience, NJ). The resulted raw FACS were then analyzed using the FlowJo (BD Bioscience, NJ) Software to determine the $CD8^+$ cell population purity.

2.4 Virtualizing T Cell Migration on 3D Collagen Matrix

3×10^5 $CD8^+$ mouse T cells with > 65% viability were resuspended in 100 µL of L-15 1% FBS medium and stained with 100 µL of 2 µM of CellTracker Green CMFDA (ThermoFisher Scientific, MA) to achieve a final concentration of 1 µM and were incubated for 5 minutes in 37˚C water bath while protected from lights. Stained T cells were washed twice using L-15 1% FBS media to remove the excess dye and centrifuged at 300 g for 5 minutes and resuspended in 250 µL of the same media. 3D collagen gel matrixes were prepared as described before, and excessive media were removed from the gel well before seeding. 3×10^5 $CD8^+$ T lymphocytes were seeded on top of the gel and gently swirled to have an evenly distributed media with cells. Seeded cells were incubated for 30 minutes at 37˚C, 5% CO_2, to allow T cells infiltration into the gel matrix. After incubation,

excessive media were removed from the gel top and washed once with 250 µL of L-15 1% FBS media to remove cells that didn't infiltrate the matrix. The collagen gel was detached from the plate using a pipette tip and carefully transferred to a 35 mm-dish using small tweezers. A small tissue harp (Warner Instrument) was placed on top of the gel to hold it down, and 5 mL of L-15 1% FBS media were added to the 35mm-dish and imaged immediately after incubation at 37˚C using the custom-build multiphoton lasering scanning microscope with a Mai Tai Ti: Sapphire laser and temperature-controlled stage insert, as described previously (Ray et al., 2018). Collagen gel and T cells were virtualized using second harmonic generation and multiphoton excitation images, respectively, at an excitation wavelength of 880 mm. Time-lapse imaging of T cell migration on 3D collagen matrix was obtained using two-channel Z-stacks of 75 µm depth at 5 µm step size for every stage position for total imaging of 45 minutes with 1.5 minutes frequency.

2.5 Pancreatic Tumor Slice Harvesting and Culturing

Fresh pancreatic tumor tissue harvested from KPCT genetically engineered mouse model were kept on ice in 1x PBS with 10 µg/ml Soybean Trypsin Inhibitor (STI) for support before slicing using a tissue vibratome (Campden Instruments, London, UK). The harvested tumor was superglued to the vibratome cutting stage with 1.5% agarose gel as support. The stage was filled with ice-cold 1X PBS for tumor slicing, and tumor tissue was sectioned at a 350 µm thickness with vibratome speed at 0.3 mm/s and frequency at 8mm. Sliced tumors were placed in sterile ice-cold 1X PBS with STI for transport. Tumor slices were carefully transferred and cultured in a 6-well or 12-well tissue culture plate with organotypic tissue culture insert (MilliporeSigma, US) coated with 3 mg/ml of rat tail collagen type 1 neutralized with 1mM HEPE in 2X PBS at a 1:1 ratio and completed with

1X PBS. Multiple slices were placed flat on 0.4 µm, 30 mm diameter cell culture inserts, while single tumor slice can be placed on 0.4 µm, 12 mm diameter cell culture inserts. Tumor slices were cultured in prewarmed RPMI 1640 supplemented with 10% FBS, 1% penicillin and streptomycin (P/S), 5 µg/mL plasmocin (Invivogen), and 10 µg/ml of STI at 37 ˚C in a 5% CO_2 humidified incubator. The tissue culture medium was changed daily, and the pancreatic tumor slices can be cultured for up to 6 days while preserving tissue integrity and cell viability.

2.6 T Cell Migration on Pancreatic Tumor Slice

2 x 10^5 mouse $CD8^+$ T cells with viability > 65% were stained with 1 µM of CellTracker Green CMFDA (ThermoFisher Scientific, MA) in L-15 media supplemented with 1% FBS as described above and washed twice in L-15 media by spinning down at 300g for five minutes. KPC tumor slices were stained with 5µM CellTracker Red CMTPX (ThermoFisher Scientific, MA) for 20 minutes and washed with RPMI. The tissue staining step was omitted for the KPCT tumor slice as the carcinoma cells can be virtualized in red fluorophore due to the presence of tdTomato. Individual tumor slice was transferred to a 12 mm organotypic culture insert in a 24-well tissue culture plate. Stained $CD8^+$ T cells were resuspended in 100 µL of L-15 media supplemented with 10% FBS, 1X P/s, 5 µg/ml Plasmocin and 10 µg/ml STI before seeded on top of the prepared tumor slice and incubated at 37 ˚C in 5% CO_2 humidified incubator for one hour. Immediately after incubation, the tumor slice was gently dipped in warm L-15 media to remove any T cells that did not infiltrate/adhere to the slice and transferred to a 35-mm tissue culture plate. A tissue harp was placed on top of the tumor slice to hold it in place during imaging. For imaging, 5 mL of warm L-15 media supplemented with 10% FBS, 1X P/S, 5 µg/ml Plasmocin and 10

µg/ml STI were added to the 35-mm culture plate. The imaging stage was set up as described before (Ray et al., 2018). Briefly, the objective lens was passed through a small hole of a square piece of parafilm and wrapped tightly with a bubble wrap to provide insulation. A 35 mm culture dish containing water prewarmed to 37 ˚C was placed on the heating element, set to 37˚C, on the microscope stage, and the objective lens was lowered to the water. The parafilm attached to the objective lens was taped to the microscope stage like a tent, and the system was allowed to equilibrate for at least 2 hours before imaging. The dish with water was replaced with the tumor sample and resealed the parafilm to maintain an even temperature. The $CD8^+$ T cells and the KPC tumor tissue/tdTomato carcinoma cells can be virtualized using multiphoton fluorescence with emission green and red, respectively, and collagen using SHG at 880-nm two-photon excitation. T cell migration was imaged at desired locations (up to two locations simultaneously) with a 75 µm deep z section with a step size of 5 µm, and images were taken in a 1.5-minute interval for up to 2 hours.

2.7 T Cell Migration Analysis

Time-lapse images of the $CD8^+$ T cells migration on 3D collagen or KPC/KPCT tumor slices were post-proceeded in Fiji, and stage drifts were corrected using the 3D correction plugin in Fiji using the SHG channel for registration. T cell movements were tracked using the Trackmate plugin in Fiji, where dynamic threshold and filters can be used to exclude erroneous tracks that might be generated by imaging artifacts or the tracking program (Tinevez et al., 2017). The post-processed cell tracking data were then analyzed by fitting to a persistent random walk model using overlapping intervals in the MATLAB model as previously described (Ray et al., 2017, 2018). Briefly, the cell's mean squared

displacement (MSD) over time interval t_i was taking from the average of all squared displacements such that:

$$\overline{x_i} = \frac{1}{n_i}\sum_{k=1}^{n_i} x_{it},$$

$$n_i = N - i + 1,$$

where n_i is the number of overlapping time intervals of duration t_i and N is the total number of time intervals. The mathematical representation of the persistent random walk model is the following:

$$MSD(t) = 2S^2P[t - P(1 - e^{-\frac{1}{P}}],$$

where S is the migration speed, and P is the persistent time. The motility coefficient can be written as such that:

$$\mu = \frac{S^2P}{n_d},$$

where n_d is the dimensionality of the random walk. For this study, the motility, speed, and persistence times for x, y, and z directions were obtained by fitting the model separately into three orthogonal directions; thus, n_d is one for each case.

The total speed of each cell can be calculated by taking the square root of the squared sum of speed in each of the three directions, x, y, and z. The equation can be written as such that:

$$S = \sqrt[2]{S_x^2 + S_y^2 + S_z^2},$$

The total motility of each cell can be obtained by adding the motility of each direction and can be written as such that:

$$\mu = \mu_x + \mu_y + \mu_z.$$

2.8 Statistic Analysis

One-way ANOVA followed by Tukey post hoc analysis was used to determine if there is a statistical difference between multiple groups, and unpaired two-way Welch's t-test was used to analyze pairwise comparisons. Due to the large sample size for each experiment, the data can be assumed to be normally distributed. All statistical analyses presented here were completed using Prism 7b (GraphPad Software, Inc) software. The difference was considered significant if $p < 0.05$.

Chapter 3: Fabrication of 3D Collagen Gel Matrix

3.1 Introduction

The ECM is a major component of the tumor stroma that plays a critical role in regulating cell and tissue function. As the most abundant ECM protein in PDAC, collagen constitutes the scaffold of the tumor microenvironment and provides structural supports and mechanical cues for resident cells (Feig et al., 2012). In addition to being a physical scaffold, recent studies have demonstrated that collagen is also actively involved in promoting tumor progression by remodeling the ECM through collagen contraction, crosslinking, and degradation to promote tumor infiltration, angiogenesis, invasion, and migration (Gong et al., 2020) . Indeed, studies have documented that the increased fibrillary collagen density is associated with increased malignancy in various human cancer types, including breast and pancreatic cancer (Acerbi et al., 2015)(P.P. Provenzano et al., 2006). PDAC has a particularly dense stroma, termed desmoplasia, where the stromal fraction can often exceed the epithelial portion of the tumor and constitute up to 90% of the total tumor volume (Xie & Xie, 2015).

3D collagen gels have long been used as *in vitro* platform for tumor invasion studies (Wolf et al., 2009). However, the traditional fabrication method often resulted in collagen nanofiber that is not representative of the invasive PDAC stroma, where collagen is remodeled into linearized and aligned fiber bundles (P.P. Provenzano et al., 2006). Therefore, methods that generate 3D collagen gel matrix that can mimic the biological environment are crucial for PDAC studies.

3.2 Fabricate 3D Collagen Gel using Cold vs. Warm media

High concentration rat tail collagen type I was purchased from Corning Life Science and stored in 4˚C refrigerator or on ice before use. 100 mM HEPE(N-(2-Hydroxyethyl) piperazine-N′-(2-ethanesulfonic acid)) in 2X PBS were added to neutralize the stock collagen solution since it is stored in 0.02N acetic acid to prevent collagen polymerization. The neutralized collagen solution was topped with either ice-cold serum-free DMEM or prewarmed (37˚C) DMEM to achieve a final concentration of 3mg/mL, a standard concentration for 3D cell culture applications. The amount of stock collagen needed was calculated using the following equation:

$$Stock\ Collagen\ Volume\ (mL) = \frac{\frac{3mg}{mL} * Desired\ Total\ Solution\ Volume\ (mL)}{Stock\ Collagen\ Concentration\ (\frac{mg}{mL})}$$

When using a standard 24-well cell culture plate, 350 µL of the mixed collagen solution was added to each well to generate a reasonably thick gel for the experiments performed in this study. The gels were left undisturbed in the hood for half an hour at room temperature to polymerize before incubating at 37˚C with 5% CO_2 overnight and then subsequently overlaid with 1 mL of DMEM. The workflow of the fabrication process is illustrated in figure 1.

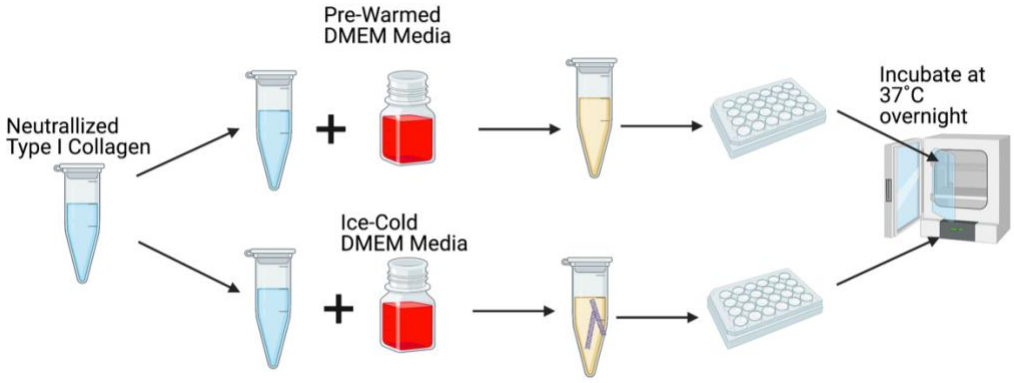

Figure 1. 3D Collagen Gel fabrication process illustration, created with BioRender.com.

3.3 Results and Discussion

Immediately after adding prewarmed DMEM media to the neutralized collagen stock solution, visible collagen fibers appeared in the mixture, while there was no noticeable fiber formation after adding the ice-cold DMEM media (Figure 1). After collagen gel polymerization, the gels were detached from the culture plate walls using a small pipette tip and carefully transferred to a 35 mm cell culture dish using tweezers for imaging. See the material and method section for detail. The collagen gels were imaged in batch to minimize variations caused by environmental and human factors. SHG images were taken at different regions of the gel to capture a more comprehensive image of the generated collagen fibers when altering the media temperature.

The collagen gels made with ice-cold media and warm media did not show any obvious difference after incubation; however, SHG images of the collagen demonstrated that while the gels made with cold media was composed of short, randomly distributed fibers (Figure 2A), the gels made with warm media produced long, aligned collagen bundles (Figure 2B) that were identical to the collagen structure seen in the KPCT tumor (Figure 2C). In

addition, although both gels were made with the same concentration of collagen (3 mg/mL), the warm media approach formed a much denser collagen network, evidenced by the SHG image as well as the number of collagen fibers extracted for the same field of view (Figure 2 D-F). One possible explanation for the observed phenomena is that higher temperature accelerated the collagen polymerization process and allowed more fiber formation.

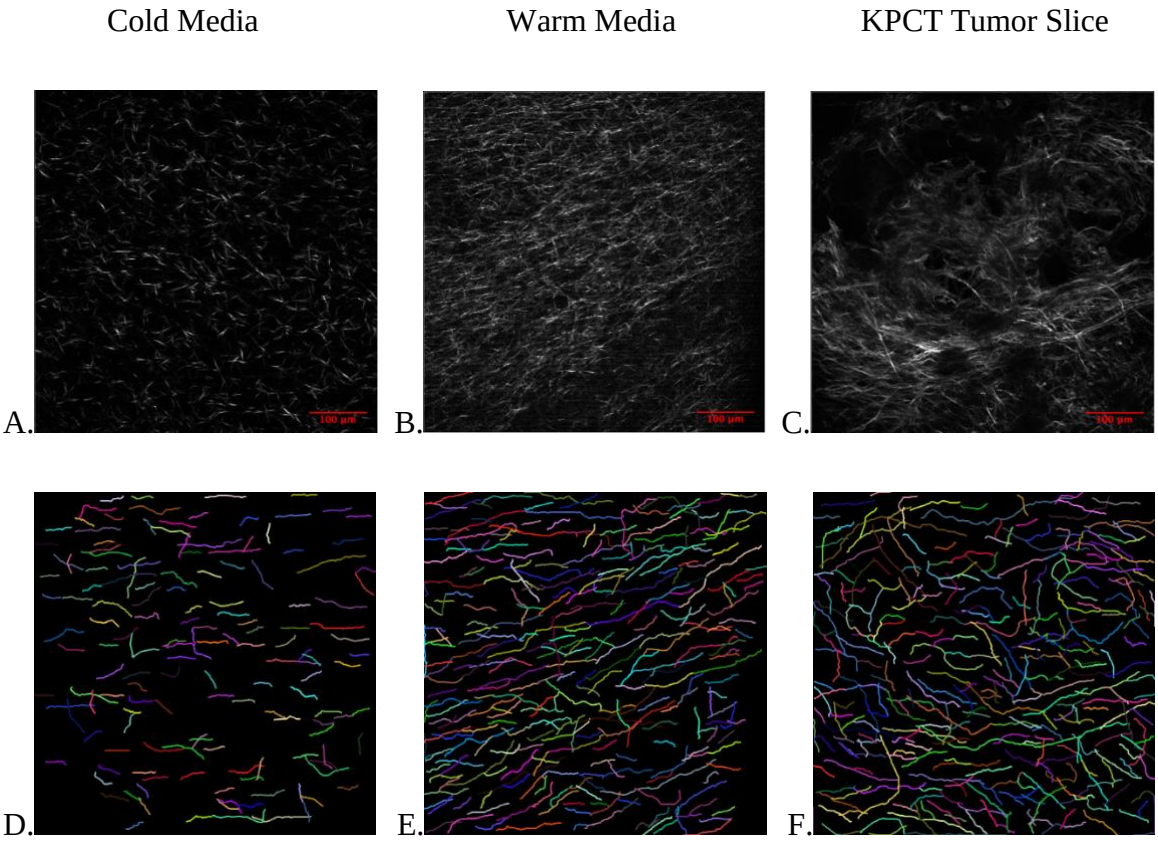

Figure 1. Collagen Fiber characterization for 3D collagen gels fabricated with ice-cold vs. prewarmed media and the collagen fibers extracted from KPCT pancreatic tumor slice. (A). SHG image of the fabricated 3D collagen gel using ice-cold media. (B). SHG image of the fabricated 3D collagen gel using prewarmed media (37˚C). All gels are made in a concentration of 3 mg/mL. (C). SHG image of the collagen fibers in the KPCT tumor slice. Scale bar: 100 µm. (D-F). CT-FIRE extracted collagen fiber overlaid image corresponding to cold media, warm media, and KPCT tumor slice, respectively, same scale.

The individual fiber properties (length, width, and alignment coefficient) of the collagen gels made with cold vs. warm media and collagen fibers extracted from tumor slices were

further analyzed using one-way ANOVA paired with Tukey *post hoc* test to determine if there were any significant differences among the three groups (Figure 3 A-C). Indeed, a significant difference in fiber length and alignment coefficient were detected between warm vs. cold media fabricated collagen gels, and tumor collagen vs. cold media fabricated collagen gels ($p<0.0001$), while no significant difference presented between warm vs. collagen fiber extracted from tumor slices ($p=0.3712$, 0.6064 for fiber length and alignment coefficient, respectively). Notably, the alignment coefficient of the collagen fibers produced using warm media is also similar to that seen in the human PDAC tumors (Drifka, 2016). However, for individual collagen fiber width, there was a significant difference among all the groups ($p<0.0001$). Although there was a significant difference in fiber width between warm media generate collagen and collagen from tumor slice, the difference was much smaller compared to that of the cold media-generated collagen fiber.

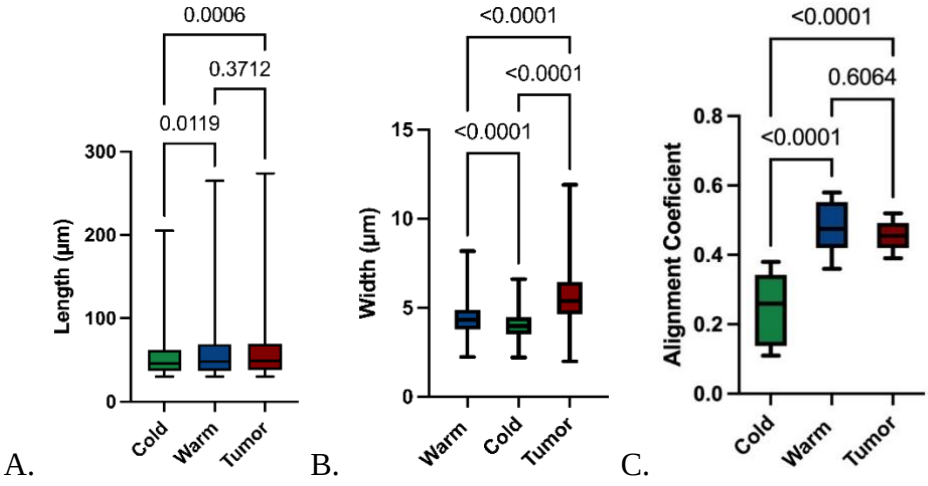

Figure 2. Statistical analysis of the collagen fiber characteristics. (A-C). Box plot of the collagen fiber length, width, and alignment coefficient in the three groups (cold media, warm media, and tumor slice), whiskers: minimum to maximum value. One-way ANOVA with Tukey post hoc test was performed to determine if the difference between multiple groups is statistically significantly different. P-value was listed on top of the corresponding plots. P<0.05 is considered significant.

3.4 Conclusion

Here we presented a rapid and easily adaptable method to produce 3D collagen matrix for cell migration study for PDAC. Using prewarmed DMEM media instead of ice-cold media leads to the production of a longer, wider, and more aligned collagen fiber network that better recapitulate the collagen structure in the PDAC tumor. The collagen structure is often remodeled during disease progression, and elevated collagen fiber alignment has been shown in the PDAC associated stroma, distinguish it from normal, and pancreatitis tissues; thus, the ability to alter fiber alignment by simple changing media temperature provides the opportunities for ex vivo studies to model different stages of PDAC. Though not performed this, the collagen gel can be imaged in 3D, and the fiber thickness can be measured using the Image J plugin "Ridge Detection" to further analyze the fiber characteristics. In addition, T lymphocyte migration studies can be performed using the two types of gels to gain insight into the dynamics of T cell migration change during different stages of PDAC.

Chapter 4: KPCT Tumor Slice as A Tool for Capturing T Cell Migration

4.1 Introduction

The 3D collagen gel matrix provides a rapid and cost-effective method that can represent the major component of the tumor ECM; however, it fails to fully recapitulate the complex tumor microenvironment that is composed of a variety of cellular and acellular components in addition to the cancer cells themselves (Feig et al., 2012). On the other hand, fresh tumor slice samples can largely resemble the architecture and cellular components of the original tumor, thus, making it a valuable tool for cell migration study to capture the dynamic interactions (X. Jiang et al., 2017). Indeed, Salmon and colleagues were able to use slice cultures to study the role played by ECM to influence T cell migration and localization in human lung tumors (Salmon et al., 2012). Furthermore, tumor slice has demonstrated its practicality in drug metabolism studies, cell biology studies, and gene therapy testing in various cancer types (Marciniak et al., 2013)(Marciniak et al., 2014)(Gerlach et al., 2014).

Tumor slice has proven to be a faithful platform for studying T cell migration in a pathologically relevant environment (X. Jiang et al., 2017). This system, coupled with nonlinear optical imaging tools like the multiphoton laser scanning microscopy (MPLSM) and second harmonic generation (SHG) imaging, provides a powerful tool to reveal the dynamic cellular interactions, especially in spatial and temporal aspects, in the 3D TME (Paolo P. Provenzano et al., 2009). MPLSM allows imaging of biological specimens at improved depth penetration and reduced photodamage by employing near-infrared femtosecond lasers to generate nonlinear signals in the visible range (Larson, 2011). By using two or more photons, MPLSM produces an emission identical to the corresponding single-photon excitation but with twice (or more) low energy, thus, decreasing

phototoxicity while maintaining a competitive resolution, similar to that of a confocal microscope (Paolo P. Provenzano et al., 2009). In addition, MPLSM can be incorporated with SHG to allow imaging of the stroma components of the TME.

From the earliest preinvasive lesion to distant metastasis, the TME plays a critical role in supporting tumor progression by inducing angiogenesis, helping malignant cells evade immune surveillance, and dictating response to therapies (Parente et al., 2018). Even though human PDAC has often been thought of as an immunologically "cold" tumor, meaning tumors that lack T cell infiltration, recent studies have revealed that human PDAC develoment can often induce immune responses that lead to increased immune cell infiltration especially cytotoxic $CD8^+$ T cells (Hartmann et al., 2014). However, even though increased cytotoxic T cell infiltration is often associated with increased patient prognosis, in the case of PDAC, most of those infiltrating T cells became trapped in the stroma and peritumoral tissues, unable to reach the cancer cells to mount an efficient immune response (Hartmann et al., 2014). The collagen-rich stroma has created a barrier for not only immune cells but also drugs to cross to efficiently eliminate the cancer cells, which is one of the major reasons why PDAC has such a poor survival rate (B. Jiang et al., 2020).

Here we validated the tumor slice platform for studying T cell migration in PDAC tumor and aim to identify whether the migration speed and motility of the $CD8^+$ T cell differ in carcinoma-rich versus stroma-rich regions of the tumor microenvironment using mouse PDAC tumor slice cultures to gain insight into the dynamic interactions between cancerous cells, immune cells, and the tumor stroma in the PDAC TME, in the hope that a deeper

understanding will help design more broadly effective immunotherapies for intractable malignancies.

4.2 KPCT Tumor Slice Preparation and Culture

The KPC mouse is a well-established and clinically important mouse model of PDAC that develops many of the same features as human PDA, such as pancreatic intraepithelial neoplasia and a robust inflammatory response with effector T cell exclusion (Hingorani et al., 2005)(Paolo P. Provenzano et al., 2012). It incorporated mutations in both KRAS and TP53 genes that are in approximately 80% and 70% of all human PDAC, respectively (Hingorani et al., 2005). The addition of tdTomato (KPCT) reporter strain to the KPC mice allows virtualization of the carcinoma cells (Figure 4), not only under fluorescence scanning but also by the naked eye. The original tumor, as well as metastatic sites, will appear reddish due to the presence of tdTomato, which allows easy identification comparing to the KPC model, where the carcinoma cells have a whitish appearance that could be difficult to distinguish. In addition, the carcinoma cells will emit a bright red fluorescence signal, eliminating the need to further stain the tumor tissue (Figure 5B).

Tumor slice can be prepared using freshly harvest PDAC tumors from KPC or KPCT genetically engineering mouse model using tissue vibratome to slice at desired thickness and cultured on collagen-coated organotypic inserts up to six days while maintaining tissue architecture and cell viability (Figure 4C). Multiple tumor slices can be placed on a 6-well culture plate, while individual slices can be placed on a 24-well plate. See method sections for detail. The slice culture media was changed daily to ensure enough nutrients were supplied to the cells.

A.  B.  C. 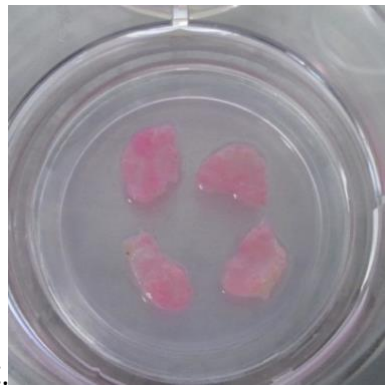

Figure 3: KPCT tumor harvesting and culture. (A). KPCT mouse bearing pancreatic tumor, distinguishable by its pink color. (B). Harvested KPCT tumor glued to the vibratome stage for slicing. A rectangular 1.5% agarose gel was used for supporting the tumor during slicing. The tumor is inherently red due to the presence of tdTomato reporter strain. (C)Sliced KPCT tumor on a coated 35 mm organoid culture insert inside a 6-well culture plate.

Time-lapse live imaging of the tumor slice using MPLSM in combination with SHG, which provides superior imaging depth and less photobleaching and phototoxic, allows the virtualization of both the carcinoma cells and the stroma collagen architecture (Figure 5). Fully activated $CD8^+$ cytotoxic T cells can be plated into the tumor slice to examine its migratory characteristics in the naïve 3D TME. The MPLSM was incorporated with a customer-build stage heater to allow live-cell imaging for days. Additionally, imaging of the whole tumor allows us to further categorize the PDAC TME into two different subtypes: carcinoma-rich region and stroma-rich region. The migration characteristics of the $CD8^+$ cells in those regions were analyzed in the following sections.

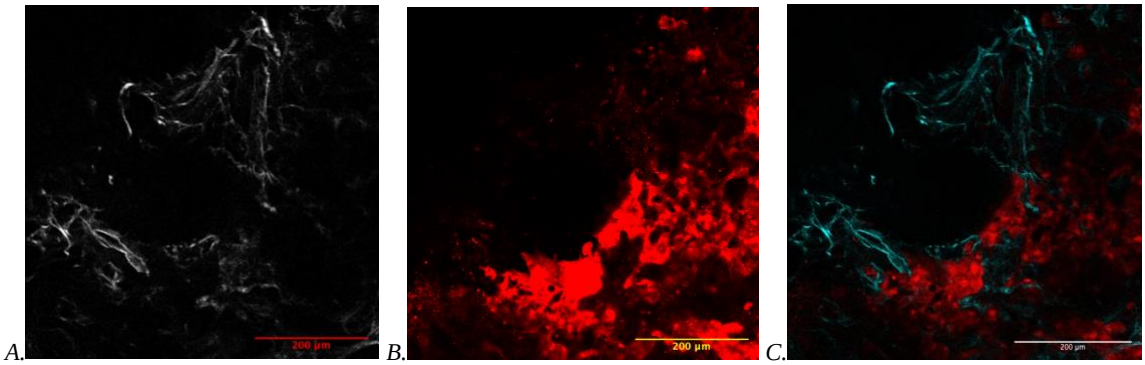

Figure 4: KPCT tumor slice imaging: (A). Representative collagen fibers in the KPCT tumor slice using SHG(B). The single representative image of PDAC carcinoma cells using multiphoton microscopy. carcinoma cells were bright right in KPCT tumor as it incorporates tdTomato in the genome. (C). Representative image of merged collagen and carcinoma cells. Collagen was post-processed to be cyan using ImageJ. Scar bar: 200 µm.

4.3 Mouse $CD8^+$ T Cell Isolation and Assessment

Cytotoxic T effector cells are fully activated $CD8^+$ T lymphocytes that have the ability to kill the cancerous cells once tumor-associated antigens are recognized. The $CD8^+$ T cells can be isolated from the spleen of the tumor-bearing KPC/KPCT mice using the EasySep Mouse CD8+ T Cell Isolation Kit and activated using the Dynabead Mouse T-Activator CD3/CD28. The purity of the isolated $CD8^+$ T cells can be assessed using flow cytometry by staining the depleted and non-depleted cell population with an anti-mouse CD8a antibody, and the unstained and non-depleted cells will serve as the negative control (Figure 6). The antibody used here were conjugated with PerCP-Cy5.5, which is a tandem fluorochrome that fluorescent at 695 nm. Therefore, the FL4 color detector channel was used for the following analysis. The result of a typic flow cytometry analysis for a $CD8^+$ T cell isolation indicated the resulted cell population was approximately 76% (Figure 6).

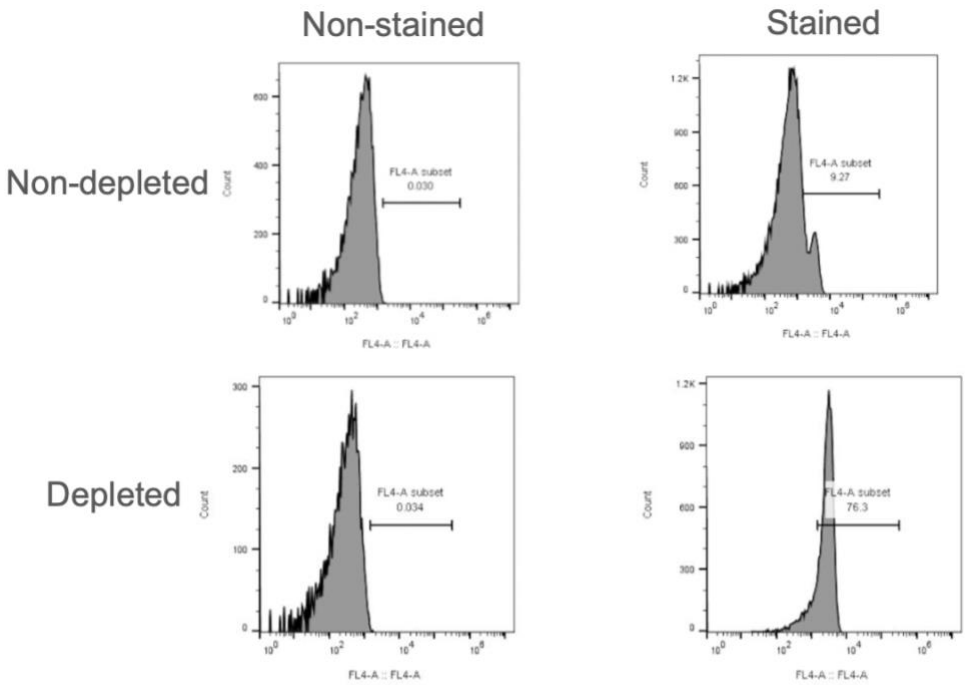

Figure 5: Flow cytometry analysis of CD8+ T lymphocyte isolation – histogram plots. Cells were stained with mouse CD8a antibody to CD8⁺ T purity. Top left: unstained and non-depleted cell population. Top right: stained and non-depleted cell population. Bottom left: unstained, depleted cell population. Bottom right: stained and depleted cell population. The same gating parameters were used for all four plots.

To allow optimal proliferation and maintain high cell viability, $1x10^5$ T cells in 50 µl of cell culture media were plated in each well of a 96-well round-bottom culture plate. Cells were allowed to aggregate and expand undisturbed for at least four days before proceeding to the next step. At least a 65% T cell viability is desired at the end of the activation period to ensure that the cells will actively attach and migrate in the 3D TME of PDAC tumor slices. If using previously frozen down T cells, the cells were allowed to recover for at least 24 hours before any subsequent experiments.

4.4 T cell Seeding and Tracking on Tumor Slice

Fully activated high viability (>65%) $mCD8^+$ T cells were first stained with CellTracker Green fluorescent dye to allow cell virtualization under MPLSM, then seeded on top of an individual KPC/KPCT tumor slice and incubated at 37˚C, 5% CO_2 for an hour to allow T cell infiltration into the tumor. T cells that did not infiltrate into the tumor were later washed off using warm media. Imaging of the T cells and tumor slice were done using MPLSM and SHG. Due to the low phototoxicity and superior imaging depth of MPLSM, T cell migration can be captured in 3D for up to 3 hours. Here, time-lapse imaging of T cell migration on tumor slice was obtained by creating a three-channel T-series (1.5-minute interval for up to 45 minutes) that incorporated with a Z-series (75 μm depth at 5 μm step-size) (Figure 4 A-B). T cell migration on the tumor slice can be tracked using the ImageJ plugin – Trackmate (Figure 4C) after correcting 3D drift by registering off with the collagen channel, which is more stable during imaging. Various filters such as quality, x/y/z axis, visibility to filtered out undesired region and spots. The tracks were then extracted and further analyzed using the persistence random walk model. See the method section for detail. By fitting to the model, T cell speed, motility, and persistence can be assessed and compared between different regions.

The method presented here serves as a promising tool to study the dynamic interaction between immune cells, cancerous cells, and the surrounding tumor stroma. Utilizing those tools can potentially help us gain insight into PDAC disease progression and metastasis as well as novel therapeutic approaches.

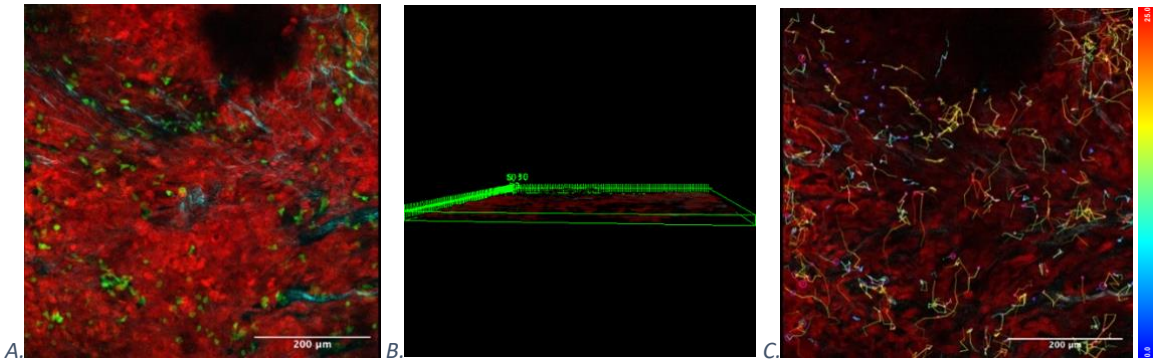

CD8⁺ T cell KPCT Tumor Cells Collagen

Figure 6:CD8+ T cell migration tracking on mouse pancreatic tumor slice. (A). Representative image of maximum intensity projection of a typical KPCT tumor slice seeded with CD8+ T cell (green). Red: carcinoma cells, cyan: collagen fiber. (B) 3D rendering view of a 75 µm z-stack of the KPCT tumor slices seeded with CD8⁺ T cell. (C): Representative image of CD8⁺ T cell migration trajectories generated using Trackmate, showing the local tracks only, track color indicates maximum velocity (lowest: blue). Scale bar: 200

4.5 T Cell Migration Differs in Different Regions of the TME

To better understand the dynamics of T cell migration in different regions of the TME, mainly carcinoma cell-rich region versus stroma-rich region, the 3D speed and motility of the plated mCD8⁺ T cells were analyzed. See the method section for detail. Generally, T cells migrate faster in the carcinoma-rich region than in the stroma-rich region (Figure 8 and movie 2-9). In fact, a majority of the T cells seem to be trapped in the dense collagen region (Figure 8 D-F), consistent with previous studies (ref.). However, it was also observed that even in the stroma-rich region of the TME, T cells migration speed could significantly improve when the collagen network is less compact and migrate along the collagen fibers via contact guidance. Though not analyzed in this study, it would be interesting to perse out this behavior and build a model to simulate the T cell migration patterns under different collagen architecture.

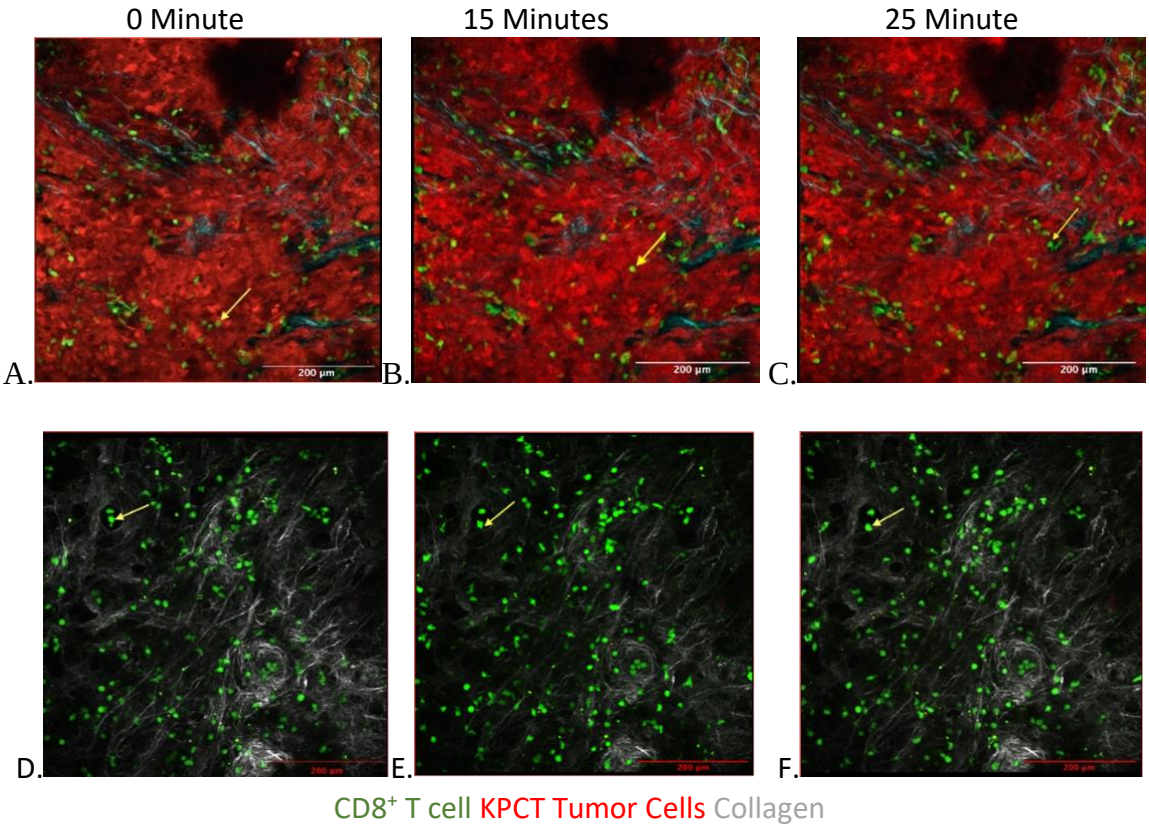

Figure 7: Representative images of CD8$^+$ T cell migration in the carcinoma-rich (Top row) and stroma-rich (bottom row) regions of the PDAC tumor microenvironment. Yellow arrow pointed at the same cell at different time points.

Bulk analysis of CD8$^+$ T cell migration in the KPCT tumor slice revealed that both the 3D speed and motility of the CD8$^+$ T cells increased significantly ($P < 0.001$ for both cases) in the carcinoma-rich region compare to that of the stroma rich region. In fact, there was almost a 2 (1.96) fold change in motility in the carcinoma-rich region with respect to that of the stroma-rich region. In addition, there was also a 36% fold change in 3D speed (data not shown).

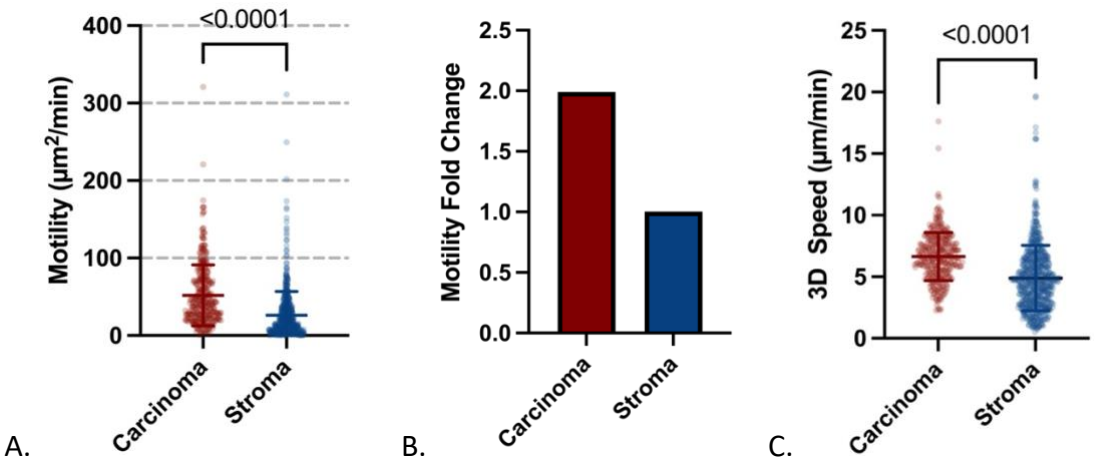

Figure 8: Statistic analysis of CD8⁺ T cell migration characteristics in the carcinoma-rich and stroma-rich regions of the KPCT TME. (A) Total motility (B). Motility fold change with respect to CD8⁺motility in the stroma-rich region. (C)3D speed. Unpaired two-way Welsch's t-test was used to determine if the difference between the two groups were significant. P values were list on the top of the corresponding groups. $P < 0.05$ is considered significant.

4.6 Discussion

T cells need to migrate efficiently into the tumor to perform their cytotoxic function to suppress tumor progression (Nicolas-Boluda & Donnadieu, 2019). The result presented here indicates that the motility and speed of T cells increased significantly in the carcinoma region compare to that in the stroma-rich region, consistent with previous migration studies done in human lung and ovarian cancers (Bougherara et al., 2015). In the 2020 study, Sadjadi and colleagues examined trajectories of human CD8⁺ T cell migration using 3D collagen gel matrixes that mimic the ECM, and they found that T cell migration pattern can be grouped into fast, slow, and mixed motility, where slow motility T cells seem to create channels through the collagen matrix and fast motility T cells use the created channels to migrate in the matrix (Sadjadi et al., 2020). In the present study, much of the

space was occupied by tumor cells in the carcinoma-rich region, but there was still a loose collagen network exist to provide structural support and critical signals for tumor cell growth. T cells plated on those regions, therefore, can utilize the loose fibers as highways to rapidly navigate and migrate through the TME. On the other, the stroma-rich regions are mainly composed of collagens, and during PDAC progression, the collagen architecture was often remodeled to elevate collagen density, which is also observed here. It can be seen that the T cells were actively trying to escape from the dense collagen region but were unable to break the collagen fiber, thus, became trapped inside, leading to low motility. If this dense stroma barrier can be broken down, it is likely to aid in the navigation and migration of the effect T cell, which could lead to increased adaptive immunity against malignant cells, thus mounting a more effective defense against the cancer progression.

4.5 Conclusion

Here we presented a method to study $CD8^+$ T cell migration in the 3D naïve PADC TME using freshly harvested pancreatic tumor from the genetically engineered mouse model, KPCT, that closely assembles many of the disease characteristics in human PDAC, including elevated collagen density. The prepared tumor slice can be cultured for up to six days in a collagen-coated organotypic culture insert, which allows $CD8^+$ harvested from the spleen of the same mouse to become fully activated. The ability to use the T cell and tumor slice from the same mouse provides a powerful tool that can fully resemble the biological changes happening during PDAC progression. Next, we aim to examine whether the migration characteristics of the $CD8^+$ T cells differ in carcinoma-rich and stroma-rich regions of the TME. Indeed, there was a statistically significant difference ($P<0.001$) in both the cell 3D speed and motility. In addition, T cells were observed to become trapped

inside dense collagen fiber, where it actively tries to escape but unable to do so. Furthermore, while dense collagen creates a barrier for T cell migration, loose collagen fibers present in the carcinoma-rich region actually aids in T cell motility and speed, probably via contact guidance. The results here are consistent with previous studies on $CD8^+$ migration in both human lung and ovarian cancer (Bougherara et al., 2015). The results here illustrate that $CD8^+$ T cells can rapidly migrate in the TME to actively search for tumorigenic cells if they can break the stroma barrier created by the dense collagen fiber network. Therefore, approaches like stroma-targeted therapy (STT) could have great potentials in advancing immune response against cancer cells and as a novel therapeutic option when using in conjecture with other treatments like chemotherapy and radiation therapy.

Chapter 5: Limitations and Future Study

Mouse PDAC tumor slices from GEMM were used as a faithful platform. However, even though mouse PDAC tumor shares many similar features with human tumor, but still cannot completely represent the autochthonous of human PDAC such that altered/additional pathways and interactions might be present in human tumor. It will be much more powerful if human PDAC tumor slice and T cells can be included in future migration studies. In addition, the T cell migration was imaged in 1.5 minutes per frame while T cells move in the second's range, resulting in gaps between cell movement that can potentially influence the accuracy of the cell tracking. One other limitation lies with the heterogeneity of the PDAC tumor tissue that has inhered variability on tumor tissue architecture. This variability can be reduced if multiple locations can be imaged at the same time on the same tumor; right now, the MPLSM stage can only image two locations within the tumor slice.

Despite the aforementioned limitation, the result from this study indicates T cell migration is largely limited by the dense collagen fibers present in the stroma, while the loose collagen fibers in the carcinoma-rich region can be exploited by T cells to navigate and migrate more efficiently in the 3D TME. Thus, stroma-targeted therapy that breaks down the stroma barrier using collagenase or hyaluronidase in combination with immunotherapy can have great potential as a novel therapeutic approach in PDAC. In addition, T cells movement in the tissue usually has been previously reported to follow a Brownian or even subdiffusive dynamics, but a switch in slow and fast motility was also observed; thus, further analysis of the interaction between T cells and carcinoma cells is wanted for understanding the dynamic migration behavior of cytotoxic T cells once a tumor antigen is

recognized. Examine the mechanism underlying the motility change can shed light on potential therapeutic approaches.

Bibliography

Acerbi, I., Cassereau, L., Dean, I., Shi, Q., Au, A., Park, C., Chen, Y. Y., Liphardt, J., Hwang, E. S., & Weaver, V. M. (2015). Human breast cancer invasion and aggression correlates with ECM stiffening and immune cell infiltration. *Integrative Biology (United Kingdom)*, *7*(10), 1120–1134. Scopus. https://doi.org/10.1039/c5ib00040h

Behrens, D., Walther, W., & Fichtner, I. (2017). Pancreatic cancer models for translational research. *Pharmacology & Therapeutics*, *173*, 146–158. https://doi.org/10.1016/j.pharmthera.2017.02.013

Bougherara, H., Mansuet-Lupo, A., Alifano, M., Ngô, C., Damotte, D., Le Frère-Belda, M.-A., Donnadieu, E., & Peranzoni, E. (2015). Real-Time Imaging of Resident T Cells in Human Lung and Ovarian Carcinomas Reveals How Different Tumor Microenvironments Control T Lymphocyte Migration. *Frontiers in Immunology*, *6*. https://doi.org/10.3389/fimmu.2015.00500

Bredfeldt, J. S., Liu, Y., Conklin, M. W., Keely, P. J., Mackie, T. R., & Eliceiri, K. W. (2014). Automated quantification of aligned collagen for human breast carcinoma prognosis. *Journal of Pathology Informatics*, *5*(1), 28. https://doi.org/10.4103/2153-3539.139707

Bredfeldt, J. S., Liu, Y., Pehlke, C. A., Conklin, M. W., Szulczewski, J. M., Inman, D. R., Keely, P. J., Nowak, R. D., Mackie, T. R., & Eliceiri, K. W. (2014). Computational segmentation of collagen fibers from second-harmonic generation images of

breast cancer. *Journal of Biomedical Optics*, *19*(1), 16007. https://doi.org/10.1117/1.JBO.19.1.016007

Burris III, H. A., Moore, M. J., Andersen, J., Green, M. R., Rothenberg, M. L., Modiano, M. R., Cripps, M. C., Portenoy, R. K., Storniolo, A. M., Tarassoff, P., Nelson, R., Dorr, F. A., Stephens, C. D., & Von Hoff, D. D. (1997). Improvements in survival and clinical benefit with gemcitabine as first- line therapy for patients with advanced pancreas cancer: A randomized trial. *Journal of Clinical Oncology*, *15*(6), 2403–2413. Scopus. https://doi.org/10.1200/JCO.1997.15.6.2403

Clark, C. E., Hingorani, S. R., Mick, R., Combs, C., Tuveson, D. A., & Vonderheide, R. H. (2007). Dynamics of the Immune Reaction to Pancreatic Cancer from Inception to Invasion. *Cancer Research*, *67*(19), 9518–9527. https://doi.org/10.1158/0008-5472.CAN-07-0175

Davies, E. J., Dong, M., Gutekunst, M., Närhi, K., van Zoggel, H. J. A. A., Blom, S., Nagaraj, A., Metsalu, T., Oswald, E., Erkens-Schulze, S., Delgado San Martin, J. A., Turkki, R., Wedge, S. R., af Hällström, T. M., Schueler, J., van Weerden, W. M., Verschuren, E. W., Barry, S. T., van der Kuip, H., & Hickman, J. A. (2015). Capturing complex tumour biology in vitro: Histological and molecular characterisation of precision cut slices. *Scientific Reports*, *5*(1), 17187. https://doi.org/10.1038/srep17187

de Kanter, R., Monshouwer, M., Meijer, D. K. F., & Groothuis, G. M. M. (2002). Precision-cut organ slices as a tool to study toxicity and metabolism of xenobiotics with

special reference to non-hepatic tissues. *Current Drug Metabolism*, *3*(1), 39–59. https://doi.org/10.2174/1389200023338071

Emmrich, J., Weber, I., Nausch, M., Sparmann, G., Koch, K., Seyfarth, M., Löhr, M., & Liebe, S. (1998). Immunohistochemical characterization of the pancreatic cellular infiltrate in normal pancreas, chronic pancreatitis and pancreatic carcinoma. *Digestion*, *59*(3), 192–198. https://doi.org/10.1159/000007488

Feig, C., Gopinathan, A., Neesse, A., Chan, D. S., Cook, N., & Tuveson, D. A. (2012). The pancreas cancer microenvironment. *Clinical Cancer Research : An Official Journal of the American Association for Cancer Research*, *18*(16), 4266–4276. https://doi.org/10.1158/1078-0432.CCR-11-3114

Gerlach, M. M., Merz, F., Wichmann, G., Kubick, C., Wittekind, C., Lordick, F., Dietz, A., & Bechmann, I. (2014). Slice cultures from head and neck squamous cell carcinoma: A novel test system for drug susceptibility and mechanisms of resistance. *British Journal of Cancer*, *110*(2), 479–488. https://doi.org/10.1038/bjc.2013.700

Goldstein, D., El-Maraghi, R. H., Hammel, P., Heinemann, V., Kunzmann, V., Sastre, J., Scheithauer, W., Siena, S., Tabernero, J., Teixeira, L., Tortora, G., Van Laethem, J.-L., Young, R., Penenberg, D. N., Lu, B., Romano, A., & Von Hoff, D. D. (2015). nab-Paclitaxel Plus Gemcitabine for Metastatic Pancreatic Cancer: Long-Term Survival From a Phase III Trial. *JNCI: Journal of the National Cancer Institute*, *107*(dju413). https://doi.org/10.1093/jnci/dju413

Gong, X., Kulwatno, J., & Mills, K. L. (2020). Rapid fabrication of collagen bundles mimicking tumor-associated collagen architectures. *Acta Biomaterialia*, *108*, 128–141. https://doi.org/10.1016/j.actbio.2020.03.019

Hafezi-Nejad, N., Fishman, E. K., & Zaheer, A. (2018). Imaging of post-operative pancreas and complications after pancreatic adenocarcinoma resection. *Abdominal Radiology (New York)*, *43*(2), 476–488. https://doi.org/10.1007/s00261-017-1378-y

Hartmann, N., Giese, N. A., Giese, T., Poschke, I., Offringa, R., Werner, J., & Ryschich, E. (2014). Prevailing Role of Contact Guidance in Intrastromal T-cell Trapping in Human Pancreatic Cancer. *Clinical Cancer Research*, *20*(13), 3422–3433. https://doi.org/10.1158/1078-0432.CCR-13-2972

Hingorani, S. R., Petricoin, E. F., Maitra, A., Rajapakse, V., King, C., Jacobetz, M. A., Ross, S., Conrads, T. P., Veenstra, T. D., Hitt, B. A., Kawaguchi, Y., Johann, D., Liotta, L. A., Crawford, H. C., Putt, M. E., Jacks, T., Wright, C. V. E., Hruban, R. H., Lowy, A. M., & Tuveson, D. A. (2003). Preinvasive and invasive ductal pancreatic cancer and its early detection in the mouse. *Cancer Cell*, *4*(6), 437–450. https://doi.org/10.1016/S1535-6108(03)00309-X

Hingorani, S. R., Wang, L., Multani, A. S., Combs, C., Deramaudt, T. B., Hruban, R. H., Rustgi, A. K., Chang, S., & Tuveson, D. A. (2005). Trp53R172H and KrasG12D cooperate to promote chromosomal instability and widely metastatic pancreatic ductal adenocarcinoma in mice. *Cancer Cell*, *7*(5), 469–483. https://doi.org/10.1016/j.ccr.2005.04.023

Jiang, B., Zhou, L., Lu, J., Wang, Y., Liu, C., You, L., & Guo, J. (2020). Stroma-Targeting Therapy in Pancreatic Cancer: One Coin With Two Sides? *Frontiers in Oncology*, *10*. https://doi.org/10.3389/fonc.2020.576399

Jiang, X., Seo, Y. D., Chang, J. H., Coveler, A., Nigjeh, E. N., Pan, S., Jalikis, F., Yeung, R. S., Crispe, I. N., & Pillarisetty, V. G. (2017). Long-lived pancreatic ductal adenocarcinoma slice cultures enable precise study of the immune microenvironment. *Oncoimmunology*, *6*(7). https://doi.org/10.1080/2162402X.2017.1333210

Kamisawa, T., Wood, L. D., Itoi, T., & Takaori, K. (2016). Pancreatic cancer. *Lancet (London, England)*, *388*(10039), 73–85. https://doi.org/10.1016/S0140-6736(16)00141-0

Lambert, A., Schwarz, L., Borbath, I., Henry, A., Van Laethem, J.-L., Malka, D., Ducreux, M., & Conroy, T. (2019). An update on treatment options for pancreatic adenocarcinoma. *Therapeutic Advances in Medical Oncology*, *11*, 1758835919875568. https://doi.org/10.1177/1758835919875568

Larson, A. M. (2011). Multiphoton microscopy. *Nature Photonics*, *5*(1), 1–1. https://doi.org/10.1038/nphoton.an.2010.2

Li, S., Xu, H.-X., Wu, C.-T., Wang, W.-Q., Jin, W., Gao, H.-L., Li, H., Zhang, S.-R., Xu, J.-Z., Qi, Z.-H., Ni, Q.-X., Yu, X.-J., & Liu, L. (2019). Angiogenesis in pancreatic cancer: Current research status and clinical implications. *Angiogenesis*, *22*(1), 15–36. https://doi.org/10.1007/s10456-018-9645-2

Liu, Y., Keikhosravi, A., Mehta, G. S., Drifka, C. R., & Eliceiri, K. W. (2017). Methods for Quantifying Fibrillar Collagen Alignment. *Methods in Molecular Biology (Clifton, N.J.)*, *1627*, 429–451. https://doi.org/10.1007/978-1-4939-7113-8_28

Marciniak, A., Cohrs, C. M., Tsata, V., Chouinard, J. A., Selck, C., Stertmann, J., Reichelt, S., Rose, T., Ehehalt, F., Weitz, J., Solimena, M., Slak Rupnik, M., & Speier, S. (2014). Using pancreas tissue slices for in situ studies of islet of Langerhans and acinar cell biology. *Nature Protocols*, *9*(12), 2809–2822. https://doi.org/10.1038/nprot.2014.195

Marciniak, A., Selck, C., Friedrich, B., & Speier, S. (2013). Mouse pancreas tissue slice culture facilitates long-term studies of exocrine and endocrine cell physiology in situ. *PloS One*, *8*(11), e78706. https://doi.org/10.1371/journal.pone.0078706

McGuigan, A., Kelly, P., Turkington, R. C., Jones, C., Coleman, H. G., & McCain, R. S. (2018). Pancreatic cancer: A review of clinical diagnosis, epidemiology, treatment and outcomes. *World Journal of Gastroenterology*, *24*(43), 4846–4861. https://doi.org/10.3748/wjg.v24.i43.4846

Nicolas-Boluda, A., & Donnadieu, E. (2019). Obstacles to T cell migration in the tumor microenvironment. *Comparative Immunology, Microbiology and Infectious Diseases*, *63*, 22–30. https://doi.org/10.1016/j.cimid.2018.12.006

Parente, P., Parcesepe, P., Covelli, C., Olivieri, N., Remo, A., Pancione, M., Latiano, T. P., Graziano, P., Maiello, E., & Giordano, G. (2018). Crosstalk between the Tumor Microenvironment and Immune System in Pancreatic Ductal Adenocarcinoma:

Potential Targets for New Therapeutic Approaches. *Gastroenterology Research and Practice*, *2018*, e7530619. https://doi.org/10.1155/2018/7530619

Provenzano, Paolo P., Cuevas, C., Chang, A. E., Goel, V. K., Von Hoff, D. D., & Hingorani, S. R. (2012). Enzymatic targeting of the stroma ablates physical barriers to treatment of pancreatic ductal adenocarcinoma. *Cancer Cell*, *21*(3), 418–429. https://doi.org/10.1016/j.ccr.2012.01.007

Provenzano, Paolo P., Eliceiri, K. W., & Keely, P. J. (2009). Multiphoton microscopy and fluorescence lifetime imaging microscopy (FLIM) to monitor metastasis and the tumor microenvironment. *Clinical & Experimental Metastasis*, *26*(4), 357–370. https://doi.org/10.1007/s10585-008-9204-0

Provenzano, P.P., Eliceiri, K. W., Campbell, J. M., Inman, D. R., White, J. G., & Keely, P. J. (2006). Collagen reorganization at the tumor-stromal interface facilitates local invasion. *BMC Medicine*, *4*. Scopus. https://doi.org/10.1186/1741-7015-4-38

Rawla, P., Sunkara, T., & Gaduputi, V. (2019). Epidemiology of Pancreatic Cancer: Global Trends, Etiology and Risk Factors. *World Journal of Oncology*, *10*(1), 10–27. https://doi.org/10.14740/wjon1166

Ray, A., Morford, R. K., & Provenzano, Paolo. P. (2018). Cancer stem cell migration in three-dimensional aligned collagen matrices. *Current Protocols in Stem Cell Biology*, *46*(1), e57. https://doi.org/10.1002/cpsc.57

Ray, A., Slama, Z. M., Morford, R. K., Madden, S. A., & Provenzano, P. P. (2017). Enhanced Directional Migration of Cancer Stem Cells in 3D Aligned Collagen

Matrices. *Biophysical Journal*, *112*(5), 1023–1036. https://doi.org/10.1016/j.bpj.2017.01.007

Rucki, A. A., & Zheng, L. (2014). Pancreatic cancer stroma: Understanding biology leads to new therapeutic strategies. *World Journal of Gastroenterology : WJG*, *20*(9), 2237–2246. https://doi.org/10.3748/wjg.v20.i9.2237

Saad, A. M., Turk, T., Al-Husseini, M. J., & Abdel-Rahman, O. (2018). Trends in pancreatic adenocarcinoma incidence and mortality in the United States in the last four decades; a SEER-based study. *BMC Cancer*, *18*(1), 688. https://doi.org/10.1186/s12885-018-4610-4

Sadjadi, Z., Zhao, R., Hoth, M., Qu, B., & Rieger, H. (2020). Migration of Cytotoxic T Lymphocytes in 3D Collagen Matrices. *Biophysical Journal*, *119*(11), 2141–2152. https://doi.org/10.1016/j.bpj.2020.10.020

Salmon, H., Franciszkiewicz, K., Damotte, D., Dieu-Nosjean, M.-C., Validire, P., Trautmann, A., Mami-Chouaib, F., & Donnadieu, E. (2012). Matrix architecture defines the preferential localization and migration of T cells into the stroma of human lung tumors. *The Journal of Clinical Investigation*, *122*(3), 899–910. https://doi.org/10.1172/JCI45817

Schneider, G., Siveke, J. T., Eckel, F., & Schmid, R. M. (2005). Pancreatic Cancer: Basic and Clinical Aspects. *Gastroenterology*, *128*(6), 1606–1625. https://doi.org/10.1053/j.gastro.2005.04.001

Seo, Y. D., & Pillarisetty, V. G. (2017). T-cell programming in pancreatic adenocarcinoma: A review. *Cancer Gene Therapy*, *24*(3), 106–113. https://doi.org/10.1038/cgt.2016.66

Siegel, R., Ma, J., Zou, Z., & Jemal, A. (2014). Cancer statistics, 2014: Cancer Statistics, 2014. *CA: A Cancer Journal for Clinicians*, *64*(1), 9–29. https://doi.org/10.3322/caac.21208

Stopczynski, R. E., Normolle, D. P., Hartman, D. J., Ying, H., DeBerry, J. J., Bielefeldt, K., Rhim, A. D., DePinho, R. A., Albers, K. M., & Davis, B. M. (2014). Neuroplastic changes occur early in the development of pancreatic ductal adenocarcinoma. *Cancer Research*, *74*(6), 1718–1727. https://doi.org/10.1158/0008-5472.CAN-13-2050

Tinevez, J.-Y., Perry, N., Schindelin, J., Hoopes, G. M., Reynolds, G. D., Laplantine, E., Bednarek, S. Y., Shorte, S. L., & Eliceiri, K. W. (2017). TrackMate: An open and extensible platform for single-particle tracking. *Methods*, *115*, 80–90. https://doi.org/10.1016/j.ymeth.2016.09.016

von Bernstorff, W., Voss, M., Freichel, S., Schmid, A., Vogel, I., Jöhnk, C., Henne-Bruns, D., Kremer, B., & Kalthoff, H. (2001). Systemic and local immunosuppression in pancreatic cancer patients. *Clinical Cancer Research: An Official Journal of the American Association for Cancer Research*, *7*(3 Suppl), 925s–932s.

Watt, J., & Kocher, H. M. (2013). The desmoplastic stroma of pancreatic cancer is a barrier to immune cell infiltration. *Oncoimmunology*, *2*(12). https://doi.org/10.4161/onci.26788

Westphalen, C. B., & Olive, K. P. (2012). Genetically engineered mouse models of pancreatic cancer. *Cancer Journal (United States)*, *18*(6), 502–510. Scopus. https://doi.org/10.1097/PPO.0b013e31827ab4c4

Wolf, K., Alexander, S., Schacht, V., Coussens, L. M., von Andrian, U. H., van Rheenen, J., Deryugina, E., & Friedl, P. (2009). Collagen-based cell migration models in vitro and in vivo. *Seminars in Cell & Developmental Biology*, *20*(8), 931–941. https://doi.org/10.1016/j.semcdb.2009.08.005

Xie, D., & Xie, K. (2015). Pancreatic cancer stromal biology and therapy. *Genes & Diseases*, *2*(2), 133–143. https://doi.org/10.1016/j.gendis.2015.01.002

Zhang, Z., Ji, S., Zhang, B., Liu, J., Qin, Y., Xu, J., & Yu, X. (2018). Role of angiogenesis in pancreatic cancer biology and therapy. *Biomedicine & Pharmacotherapy*, *108*, 1135–1140. https://doi.org/10.1016/j.biopha.2018.09.136

Appendix

Appendix A: Videos

Time Lapse microscopy videos referred to in the thesis can be found in this link. For description of each movie, refer to “List of videos”.